特集 Road Border Recognition Using FIR Images and LIDAR Signal Processing *

高木聖和 Kiyokazu TAKAGI
バーゼル ファルディ Basel Fardi
ヘンドリック ヴァイゲル Hendrik Weigel
ゲルド ヴァニーリック Gerd Wanielik

This paper addresses the detection and tracking of road borders in non-cooperative environments. A 2-dimensionalscanning LIDAR is used to improve the reliability of the FIR camera based road border recognition. In order to detect the road boarders we apply a Kalman-filter based model fitting strategy. Extracted measurements of the FIR images are transformed into the vehicle coordinate system in order to provide a precise description of the road course ahead. The model description ina common coordinate system - the vehicle coordinate system- allows an easy compensation of the ego-motion and a direct and straight forward fusion of the different sensor data. Both the detection and the estimation were developed and enhanced for the intended sensor configuration. The corresponding mathematical derivations are presented in this paper. Using the range values, delivered by the LIDAR, a more stable estimation of the pitch angle can be achieved. The realization of that is shown in detail. This is used to define the ROI in which the image processing is carried out.

1. INTRODUCTION

Investigations about lane road detection systems resp. Have already been carried out for more than two decades (the references[1)-4)]). Mostly, a video vision based system detects and tracks the road markings and/or boundaries. Such approaches have impressive results in cooperative areas under good weather conditions. In contrast to that FIR sensors turn out their strength and benefits mainly under nocturnal conditions within noncooperative environments. In comparison with video sensors the high tolerance towards different light conditions makes a FIR sensor also suitable for scenarios with extremly difficult light conditions like shadow or back-light.

FIR cameras are recently used for Advanced Driver Assistance Systems (ADAS) in passenger cars. HONDA and BMW optionally prepare a FIR camera system for their flagship car and especially the HONDA system also recognizes pedestrians. LIDAR sensors are installed instead of a radar for ACC functionality or as a pre-crash system. TOYOTA and NISSAN have been using the LIDAR for their ADAS such as ACC. SUBARU employs the LIDAR for all-speed ACC on their vehicle in 2006.

Although not indented for a commercial application so far LIDAR systems are also used for lane recognition purposes. In the reference[5)] a 2-dimensional scanning LIDAR detects the reflecting lane markings. The reference[6)] uses a one layer LIDAR for the detection and tracking of the road borders without the need of the existence of lane markers. LIDARs are similar unattached to different light conditions like FIR cameras. Moreover, as an active sensor the LIDAR measures distances directly and therefore more precisely than vision based sensors.

2. THE COMBINED SENSOR SYSTEM

Taking the advantages of both sensors into account a combination could lead to an improved and more reliable system for road border tracking. As mentioned above each sensor as stand-alone system is able to fulfill a desired DAS functionality. So, a road boarder detection would not lead to additional hardware costs. Already existing algorithms like object recognition[9)] will also be used.

Figure 1 gives an overview of the road border tracking system. A stand-alone approach using the FIR camera will be described in the next section. The LIDAR improves the basic system. It sustains the road boarder recognition within the overall system in different ways. The LIDAR emits the laser beam forward with 2-dimensional scanning by the rotating hexagon mirror to detect the forward objects of the egovehicle. The mass-produced LIDAR only uses the upper 3 mirrors to detect ahead vehicles for ACC system but in our system we also use the lower 3 mirrors (see Fig. 2). As

* Reprinted with permission from Intelligent Vehicles Symposium, 2007 IEEE Digital Object Identifier: 10. 1109/IVS. 2007. 4290294 Publication Year: 2007, Page(s): 1278-1283

shown in Fig. 3 these specifications, except the elevation field of view, are the same as the mass-production type. The LIDAR signal processing supports the FIR processing at different points:

- First, with the output of a object tracking algorithm we exclude regions from the ROI which are overlayed by other objects[9].
- With the lower 3 layers a pitch angle estimation is done to improve the transformation between vehicle coordinate system and image plane.
- Depending on ego-vehicle position on the road a combined range and reflectivity signal processing distinguishes if the scanned area is on or beside the road. A detailed explanation of the reflectivity signal processing and its usage concerning the detection of the road area can be found in the reference[6].

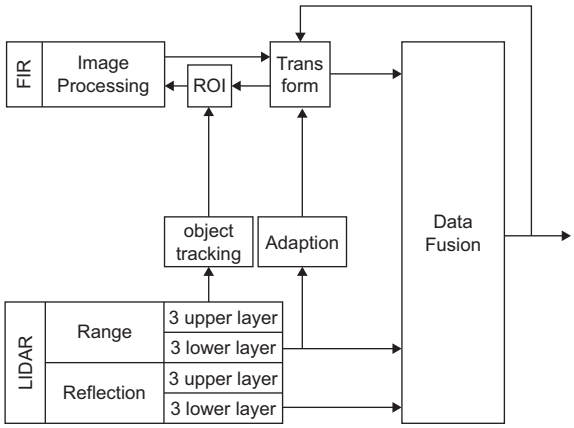

Fig. 1 Scheme of the overall system

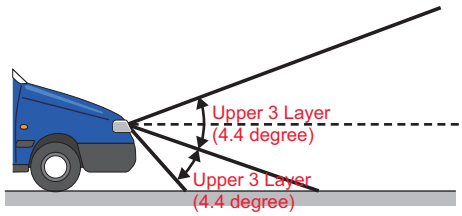

Fig. 2 Detection angle (elevation angle)

Item	Specification
Range	120 m
Azimuth Field of View	-18...18 deg
Elevation Field of View	-4...4 deg
Caluculation frequency	10 Hz
Horizontal Resolution	0.08 deg.
Size	W100*H60*D80

Fig. 3 Specifications of the LIDAR

3. ROAD BORDER DETECTION IN FIR IMAGES

In this section a complete approach for solving the problem of the road border detection in FIR-images is presented. The way, how to increase the robustness of this approach with the help of the multi layer LIDAR will be discussed in the next section.

Before going more into detail, it is useful to introduce the most important properties of the FIR-imaging regarding the intended application.

- The textural difference between the road surface and the surrounding area in FIR-images is usually very poor.
- The road border can mostly be recognized as some discontinuities in the FIR-image.
- The FIR-images are sometimes very noisy depending on the weather condition. Since such noise appears as variations of the image structure, it can cause some difficulties during the detection process.
- Further objects (pedestrians, trees, crash barriers etc.), which occur near to the road border, can also cause some difficulties because of the corresponding gray-scale variations.

Taking these items into account we extended our road border detection algorithms introduced in the reference[6] and[7] at different points. In both systems we followed a model fitting strategy, in which the road border is approximated by means of a geometric curve. Such approach shows robustness against noise and interruptions. The procedure of the associated processing is typically subdivided into two steps: measurements extraction and model parameter estimation. Using the Kalman-Filter approach and the vehicle coordinate system in order to describe the road curve, we are able to compensate the ego motion and to give an exact estimation of the road border. The way how to consider the ego motion in the estimation process is one of the enhancements presented in this paper. With it the processing is significantly simplified without restricting the suitability of the method. The second point of our enhancements is the usage of the local orientation in the image plane in order to increase the reliability of the measurements. Therewith a lot of irrelevant measurements caused by other objects can easily be excluded. With the help of the structure tensor method the local orientation can be measured on the one hand and on the other hand we are able to distinguish between gray-scale variations caused by noise and discontinuities corresponding to relevant image structures. The use of such a method in the extraction of

measurements is also one of the important extensions of our algorithms.

A. Model parameter estimation

As mentioned above a Kalman-Filter approach is used to estimate the parameters of a predetermined curve describing the road border. Because of the intended data fusion of different sensors, measuring and estimating domains are completely separated. While the vehicle coordinate system ${}^{v}x$ defines a common domain, in which the curve parameters are estimated, the measuring domains are different depending on the measuring principle of the sensors. In the case of the FIR camera the measuring domain is the image plane ${}^{i}x$ and the transition into the estimating domain is non-linear. We denote this transition f_c and the transition between two time steps f_a.

To estimate the curve of the road on the basis of the measurements of the FIR-camera and the LIDAR, a functional model is considered. A curve with constant curvature, a circle, is chosen. It suits for the typical distances, which can be observed by the LIDAR in our application as well as for the set of distances, for which the position of the road border is measured in the FIR-camera image. The original model equation is transformed into a form suitable for the estimation purposes. It is adapted with the help of a shift in the y-axis (y_0) and a correction term of the curvature parameter c representing the line position of the left (i=1) or right (i=0) road boarder:

$$\left(\frac{1}{c} - b \cdot i\right)^2 = {}^{v}x^2 + \left({}^{v}y - \frac{1}{c} + {}^{v}y_0\right)^2 \quad \cdots\cdots\cdots (1)$$

The sign of the radius $\frac{1}{c}$ respects the direction of the curve. In the simple case we can accept that the vehicle moves along the circle segment with the radius and the deviation from the initial orientation of the vehicle is modelled as noise of the state parameters. The state vector in this case consists of the three parameters describing our circle model: c, b and y_0. To get some predictions in order to perform the update step of the Kalman-Filter, a set of distances ${}^{v}x_n$ is determined and put in the last equation. The corresponding ${}^{v}y_n$-coordinates can be computed if the equation is converted into a form where ${}^{v}y$ is a function of the chosen distance ${}^{v}x$ as well as of the parameters contained in the state vector:

$${}^{v}y_{1,2} = \frac{1}{c} - {}^{v}y_0 \mp \sqrt{\left(\frac{1}{c} - b \cdot i\right)^2 - {}^{v}x^2} \quad \cdots\cdots\cdots (2)$$

Finally, the correct solutions and the corresponding ${}^{v}x_n$ are transformed into the image plane to obtain a new estimation of the model parameters. However, this assumption leads to an inaccurate fitting if the orientation of the vehicle deviates from the assumed orientation significantly. Therefore we make this quantity deterministic and estimate it with the model parameters. The state vector turns out to be:

$$x^T(t_k) = ({}^{c}c(t_k), {}^{c}b(t_k), {}^{c}y_v(t_k), {}^{c}\gamma_v(t_k)) \quad \cdots\cdots\cdots (3)$$

where ${}^{c}y_v(t_k)$ is the offset parameter indicating the shift in the y-axis. All of the parameters are described now in a circle coordinate system, which is introduced to describe the relative position of the vehicle with regard to the circle (**Fig. 4**).

To simplify the processing we correct the relative position of the coordinate systems ${}^{c}x$ and ${}^{v}x$ by considering the ego motion[1] at each time step, when the estimation is performed. An additional offset ${}^{c}x_v$ should be avoided. In the first step the prediction step of the Kalman-Filter is carried out in the current circle coordinate system, where the state ${}^{c(tk\text{-}1)}x_v(t_{k\text{-}1}) = 0$, ${}^{c}y_v = {}^{c(tk\text{-}1)}y_v(t_{k\text{-}1})$ and ${}^{c}\gamma_v = {}^{c(tk\text{-}1)}\gamma_v(t_{k\text{-}1})$ is taken as a starting point. Using the actual velocity ${}^{c(tk\text{-}1)}y_v(t_{k\text{-}1})$ and turn rate ${}^{c(tk\text{-}1)}\dot{\gamma}v(t_{k\text{-}1})$ of the vehicle we obtain for the next time t_k and the time interval T the following interim state:

$$\begin{pmatrix} {}^{c(t_{k-1})}x_v(t_k) \\ {}^{c(t_{k-1})}y_v(t_k) \\ {}^{c(t_{k-1})}\gamma_v(t_k) \end{pmatrix} = \begin{pmatrix} {}^{c(t_{k-1})}x_v(t_{k-1}) + a_1a_3 - a_2a_4 \\ {}^{c(t_{k-1})}y_v(t_{k-1}) + a_2a_3 - a_1a_4 \\ {}^{c(t_{k-1})}\gamma_v(t_{k-1}) + {}^{c(t_{k-1})}\dot{\gamma}_v(t_{k-1}) \cdot T \end{pmatrix} \quad \cdots (4)$$

with

$$a_1 = \cos\left({}^{c(t_{k-1})}\gamma_v(t_{k-1})\right)$$

$$a_2 = \sin\left({}^{c(t_{k-1})}\gamma_v(t_{k-1})\right)$$

$$a_3 = \frac{{}^{c(t_{k-1})}V_v(t_{k-1}) \sin\left({}^{c(t_{k-1})}\dot{\gamma}_v(t_{k-1}) \cdot T\right)}{{}^{c(t_{k-1})}\dot{\gamma}_v(t_{k-1})}$$

$$a_4 = \frac{{}^{c(t_{k-1})}V_v(t_{k-1}) \left(1 - \cos\left({}^{c(t_{k-1})}\dot{\gamma}_v(t_{k-1}) \cdot T\right)\right)}{{}^{c(t_{k-1})}\dot{\gamma}_v(t_{k-1})}$$

The movement of the vehicle is accompanied by the movement of the tangential circle coordinate system afterwards. Lastly, the new position of the vehicle has to be transformed into the new circle coordinate system and has to be expressed again with the state space variables described above. We assume that both the radius of the circle and the width of the road remain unchanged during the prediction step:

[1]The ego motion is measured by means of additional sensors.

$$ {}^{c}c\ (t_k) = {}^{c}c\ (t_{k-1}),\ {}^{c}b\ (t_k) = {}^{c}b\ (t_{k-1}) \quad \cdots\cdots\cdots\cdots (5) $$

The new offset parameter is calculated using the position parameters ${}^{c(tk-1)}x_v\ (t_k)$ and ${}^{c(tk-1)}y_v\ (t_k)$:

$$ {}^{c}y_v\ (t_k) = \frac{1}{{}^{c}c\ (t_{k-1})} - \sqrt{{}^{c(t_{k-1})}x_v^2\ (t_k) + \left(\frac{1}{{}^{c}c\ (t_{k-1})} - {}^{c(t_{k-1})}y_v\ (t_k)\right)^2} \quad \cdots\cdots (6) $$

And the new angle parameter is delivered by

$$ {}^{c}\gamma_v\ (t_k) = {}^{c(t_{k-1})}\gamma_v\ (t_k) - \arctan \frac{{}^{c(t_{k-1})}x_v\ (t_k)}{\frac{1}{{}^{c}c\ (t_{k-1})} - {}^{c(t_{k-1})}y_v\ (t_k)} \quad \cdots (7) $$

This two equations together with the parameters ${}^{c}c\ (t_k)$ and ${}^{c}b\ (t_k)$ are the elements of the vector f_a. The way to define the vector f_c is discussed in the next subsection.

B. Extraction of measurements

The extraction of measurements from the FIR-images is normally achieved by detecting the significant grayscale variations, which occur around the predicted curve. As mentioned in the last section in our system we consider further properties of the image structure in order to increase the reliability of the estimation. On the one hand we distinguish between noise and relevant grayscale variations, on the other hand the orientation of the local image structure is additionally taken into account. Using the structure tensor approach[8] both properties can be detected.

The structure tensor is a symmetric 2 × 2 matrix J, and its components are defined as follows:

$$ J_{pq}\ (x) = \int_{-\infty}^{\infty} \omega\ (x - x') \left(\frac{\partial g\ (x')}{\partial x'_p}\ \frac{\partial g\ (x')}{\partial x'_q}\right) d^2x' \quad \cdots (8) $$

The vector x contains the coordinates of a pixel in the image $g\ (x)$, and ω is the window function which determines the size and shape of the neighborhood around the pixel. Through a rotation of the coordinate system, the structure tensor is brought into a diagonal form with eigenvalues J'_{11} and J'_{22}. The orientation is given by the rotation angle and computed as

$$ \phi = \frac{1}{2} \arctan \frac{2J_{12}}{J_{22} - J_{11}} \quad \cdots\cdots\cdots\cdots\cdots\cdots (9) $$

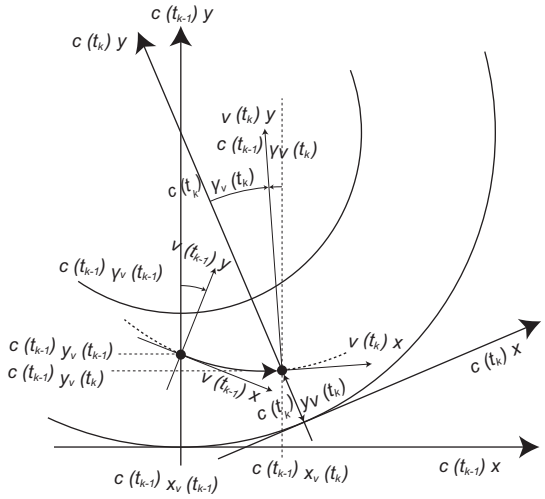

Fig. 4 Functional road model and the vehicle prediction steps

The classification of the image pixels as homogeneous, isotropic or oriented is performed by the interpretation of the eigenvalues as follows:

- Homogeneous, $J'_{11} = J'_{22} = 0$:

$$ J'_{11} + J'_{22} < C_h \quad \cdots\cdots\cdots\cdots\cdots\cdots\cdots\cdots (10) $$

where the threshold Ch is determined by the noise level in the image

- Isotropic, $J'_{11} = J'_{22} \neq 0$:

$$ J'_{11} + J'_{22} > C_h \cap \frac{J'_{11} - J'_{22}}{J'_{11} + J'_{22}} < C_i \quad \cdots\cdots\cdots\cdots (11) $$

- Oriented, $J'_{11} = J'_{22} = 0$:

$$ J'_{11} + J'_{22} > C_h \cap \frac{J'_{11} - J'_{22}}{J'_{11} + J'_{22}} > C_i \quad \cdots\cdots\cdots\cdots (12) $$

To create uniformly distributed predictions in the image plane we define the ${}^{v}x$-coordinates with the help of a nonlinear geometric series:

$$ {}^{v}x\ (n) = {}^{v}x_{min} + \Delta^{v}x_0 \cdot \frac{k^{n-1} - 1}{k - 1} \quad \cdots\cdots\cdots\cdots (13) $$

where ${}^{v}x_{min}$ is an offset according to the displacement of the camera in the vehicle coordinate system. This parameter and the initial distance $\Delta^{v}x_0$ as well as k are determined

empirically. The corresponding ${}^{v}y$-coordinates can be defined using the model equation

$$({}^{v}x - {}^{v}x_m)^2 + ({}^{v}y - {}^{v}y_m)^2 = \left(\frac{1}{c} - b \cdot i\right)^2 \quad \cdots\cdots\cdots (14)$$

where ${}^{v}x_m$ and ${}^{v}y_m$ are the center coordinates of the circles in the vehicle coordinate system:

$${}^{v}x_m = \left(\frac{1}{c} - {}^{c}y_v\right) \sin {}^{c}\gamma_v \quad \cdots\cdots\cdots (15)$$

$${}^{v}y_m = \left(\frac{1}{c} - {}^{c}y_v\right) \cos {}^{c}\gamma_v \quad \cdots\cdots\cdots (16)$$

The ${}^{v}y$-coordinates are then obtained by converting the equation 14:

$${}^{v}y(i,n) = {}^{v}y_m - \mathrm{sign}(c) \sqrt{\left(\frac{1}{c} - b \cdot i\right)^2 - ({}^{v}x(n) - {}^{v}x_m)^2} \quad \cdots (17)$$

where the sign of the root depends on the sign of the curvature. The related components of the f_c-vector are then given by the perspective projection equations:

$${}^{i}x = \left[\frac{{}^{ca}x}{{}^{ca}z} f + \frac{ddx}{2}\right] \frac{N_x}{ddx} \quad \cdots\cdots\cdots (18)$$

$${}^{i}y = \left[\frac{{}^{ca}y}{{}^{ca}z} f + \frac{ddx}{2}\right] \frac{N_y}{ddy} \quad \cdots\cdots\cdots (19)$$

where $N_x \times N_y$ is the number of the pixels, f the focal length, (ddx;ddy) the sensor dimension and

$${}^{ca}x = D_x \cdot D_y \cdot D_z \cdot [{}^{v}x - {}^{v}x_{ca}] \quad \cdots\cdots\cdots (20)$$

is the transformation into the camera coordinate system with the help of the rotation matrices and the translation vector describing the camera position in the vehicle coordinate system.

To define the component of f_c regarding the local orientation we introduce a set of auxiliary points, which is created by means of the tangential vectors at the points (${}^{v}x$ (i;n); ${}^{v}y$ (i;n)) (**Fig. 5**). The tangential vector is defined as follows:

$${}^{v}d = \begin{pmatrix} {}^{v}d_x \\ {}^{v}d_y \end{pmatrix} = \begin{pmatrix} \mathrm{sign}(c)\,({}^{v}y_m - {}^{v}y) \\ \mathrm{sign}(c)\,({}^{v}x - {}^{v}x_m) \end{pmatrix} \quad \cdots\cdots\cdots (21)$$

Its transformation into the camera coordinate system can be performed in consideration of the camera rotation:

$${}^{ca}d = D_x \cdot D_y \cdot D_z \cdot {}^{v}d \quad \cdots\cdots\cdots (22)$$

and the corresponding auxiliary point turns out to be:

$${}^{ca}x_t = {}^{ca}x + {}^{ca}d \quad \cdots\cdots\cdots (23)$$

Now we can supply the last component of fc by transforming both of the points into the image plane and by giving the slope defined between them:

$$\tan {}^{i}\varphi = \frac{{}^{i}y - {}^{i}y_t}{{}^{i}x_t - {}^{i}x} = \frac{\left(\frac{{}^{ca}y}{{}^{ca}z} f + \frac{ddy}{2}\right)\frac{N_y}{ddy} - \left(\frac{{}^{ca}y_t}{{}^{ca}z_t} f + \frac{ddy}{2}\right)\frac{N_y}{ddy}}{\left(\frac{{}^{ca}x_t}{{}^{ca}z_t} f + \frac{ddx}{2}\right)\frac{N_x}{ddx} - \left(\frac{{}^{ca}x}{{}^{ca}z} f + \frac{ddx}{2}\right)\frac{N_x}{ddx}} \quad \cdots (24)$$

$${}^{i}\varphi = \arctan\left[\frac{N_y ddx\,({}^{ca}y\,{}^{ca}d_z - {}^{ca}z\,{}^{ca}d_y)}{N_y ddy\,({}^{ca}z\,{}^{ca}d_x - {}^{ca}x\,{}^{ca}d_z)}\right]$$

4. LIDAR BASED PITCH ANGLE COMPENSATION

The analysis of the FIR images regarding road border detection in non cooperative areas has shown that for an efficient extraction of relevant features it is necessary to restrict the processing on small areas close to the road borders. These regions of interest are determined using the curve parameters which are estimated in the last fusion step. This is illustrated in **Fig. 1** with the feedback-branch. For an accurate placement of the regions of interest in the image, the transformation parameters between vehicle coordinate system and image plane must be adapted for each time step. This is performed with the help of the pitch angle which is determined using the range measurements of the laser scanner: In front of the host vehicle the 3 lower layers hit the road surface in a distance between 5 and 12 meters. For a dedicated lateral span (in accordance with the vehicle width of 1.7 meters) a line for each layer is calculated. This is also done during the initial calibration process. A displacement of these lines is related to the change of the pitch angle. **Figure 6** shows an example of the distance measurement of the first and second layer. Depending on the current pitch angle not all lower layers can be used always. As the LIDAR is attached on the right side of the front bumper the used distance

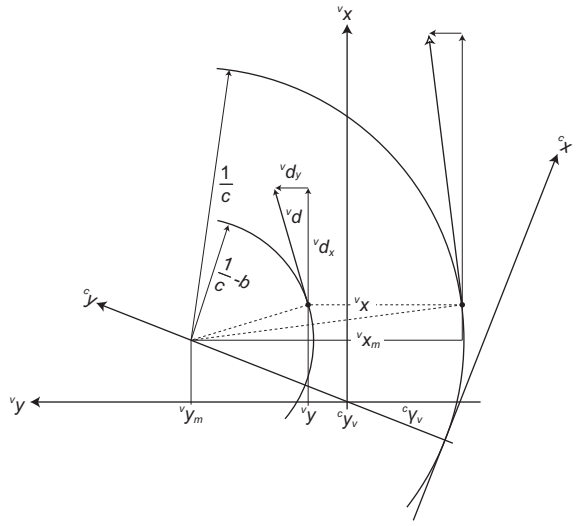

Fig. 5 Determination of the tangential vector

measurements (with lines connected points) lie between -0.4 and 1.3 meters. The points cluster on the right indicates the road edge. For each layer the line is computed and plotted in **Fig. 6** with the corresponding color. Local irregularities on the road surface could bastardize this computation. To avoid such mistakes an 'overall' line (bold black one) is calculated and applied for the pitch angle compensation. Furthermore the updated transformation matrix is used to calculate the correct reference point in vehicle coordinates for every road border detection in the image plane. The method how to determine the pitch angle is explained below.

The **Fig. 7** illustrates the position S of a mounted sensor in the vehicle as well as the geometric measures at the initial position of the vehicle. The origin of the vehicle coordinate system is located below the rear axle. The point D represents an arbitrary defined rotation axis, which must be unchanged. The length of the vector r and the angle γ are also constant and they are calculated by the values of the initial position (denoted by the index 0):

$$r_0 = |r_0| = |r_{s0} - r_D| = \text{const} \quad \cdots\cdots\cdots\cdots\cdots\cdots (25)$$

$$\gamma = \arccos\left(\frac{-r_0 \cdot l_0}{r_0 \cdot l_0}\right) = \text{const} \quad \cdots\cdots\cdots\cdots\cdots\cdots (26)$$

where

$$l_0 = \begin{pmatrix} \sqrt{l_0^2 - r_{s0z}^2} \\ -r_{s0z} \end{pmatrix} \quad \cdots\cdots\cdots\cdots\cdots\cdots\cdots\cdots (27)$$

is the distance measurement which results from the range detection in the initial position. The rotation angle of the sensor at the *y* axis in the initial state is calculated by:

$$a_0 = \arcsin\left(\frac{r_{S0z}}{l_0}\right) \quad \cdots\cdots\cdots\cdots\cdots\cdots\cdots\cdots (28)$$

with the help of the vector *r*, the angle γ and the measured distance l delivered by the range detection, the current pitch angle can be calculated as follows:

$$\Delta a = a - a_0 \quad \cdots\cdots\cdots\cdots\cdots\cdots\cdots\cdots (29)$$

$$a = \beta + \delta = \arcsin\left(\frac{r_0}{s}\sin\gamma\right) + \arcsin\frac{r_{Dz}}{s} \cdots\cdots (30)$$

and

$$s = \sqrt{r_0^2 + l^2 - 2r_0 l\cos\gamma} \quad \cdots\cdots\cdots\cdots\cdots\cdots (31)$$

And so the pitch angle $\Delta\alpha$ can be used to calculate the actual translation vector r_s and the current rotation matrix R_y:

$$r_s = r_D + \begin{pmatrix} \cos\Delta a & \sin\Delta a \\ -\sin\Delta a & \cos\Delta a \end{pmatrix} (r_{s0} - r_D) \quad \cdots\cdots (32)$$

$$R_y = \begin{pmatrix} \cos(\varphi_y + \Delta a) & 0 & -\sin(\varphi_y + \Delta a) \\ 0 & 1 & 0 \\ \sin(\varphi_y + \Delta a) & 0 & \cos(\varphi_y + \Delta a) \end{pmatrix} \cdots\cdots (33)$$

Consequently, the new relative position of the sensor can be completely described and the transformation of a point from the vehicle coordinate system into the camera coordinate system turns out to be:

$${}^{ca}x = D_x \cdot D_y \cdot D_z \cdot \left({}^{v}x - \begin{pmatrix} r_{sx} \\ r_{sy} \\ r_{sz} \end{pmatrix}\right) \quad \cdots\cdots\cdots\cdots\cdots (34)$$

5. RESULTS

The introduced approach was tested with selected off-line scenarios and under real environment conditions. It turned out that the LIDAR based pitch angle compensation is an appropriate solution to deal with the often very warped road surfaces in non cooperative environment. **Figure 8** presents some examples of processed FIR images and the corresponding tracking results. The lower row presents the result of the detection step (8), where the color denotes the orientation of the grey scale variation (9). The computation of the complete image is just done for visualization purposes.

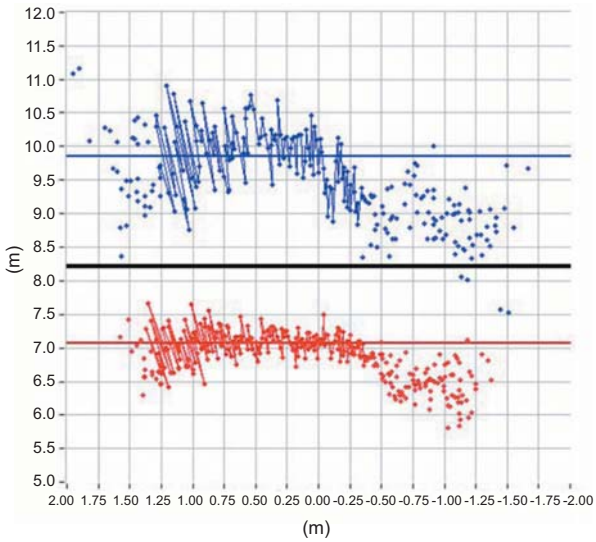

Fig. 6 Example of the distance of the 1st and 2nd layers measured by the LIDAR

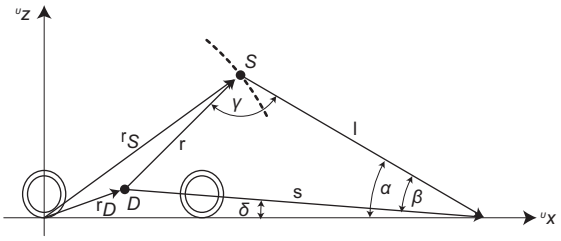

Fig. 7 Geometric relations of the sensor and vehicle coordinates

Actually, the algorithm computes only the image region under the horizon to save computation resources. The upper row shows the original images overlayed with the measurements for the update step of the Kalman-Filter. As can be seen, the usage of the orientation provides a reliable way to pick out image points belonging to the road border. Consequently the achieved estimation of the model parameters resp. the road borders is very precise.

REFERENCES

1) E.D. Dickmanns, B.D. Mysliwetz, “Recursive 3D road and relative ego-state recognition” IEEE Trans. Pattern Analysis and Machine Intelligence, Vol. 14, No.2, Feb. 1992, pp. 199-213.
2) R. Wang, Y. Xu, Libin, Y. Zhao, “A Vision Based Road Edge Detection Algorithm,” Proc. IEEE Internatonal Conference on Intelligent Vehicles, Versailles, 2002.
3) N. Apostoloff, A. Zelinski, “Robust vision based Lane Tracking using Multiple Cues and Particle Filtering,” Proc. IEEE Internatonal Conference on Intelligent Vehicles, pp. 558-563, 2003.
4) R. Chapuis, R. Aufrere, F. Chausse, “Accurate Road Following and Reconstruction by Computer Vision” IEEE Trans. Intelligent Transportation Systems, vol. 3, no.4, pp. 261-270, December 2002.
5) T. Ogawa, K. Takagi, “Lane Recognition Using On-vehicle LIDAR” Proc. IEEE Intelligent Vehicles Symposium, 2006.
6) B. Fardi, U. Scheunert, H.Cramer, G. Wanielik, “Multi Modal Detection and Parameter-based Tracking of Road Borders with a Laser Scanner” Proc. IEEE Intelligent Vehicles Symposium, 2003.
7) B. Fardi, G.Wanielik, “Hough Transformation Based Approach for Road Border Detection in Infrared Images” Proc. IEEE Intelligent Vehicles Symposium, 2004.
8) B. J¨ahne, “Digital Image Processing. Concepts, Algorithms, and Scientific Applications”, Springer-Verlag, Berlin, Heidelberg, New York, 2002.
9) K. Takagi, K. Morikawa, T. Ogawa, M. Saburi, “Road Environment Recognition Using On-vehicle LIDAR” Proc. IEEE Intelligent Vehicles Symposium, 2006.

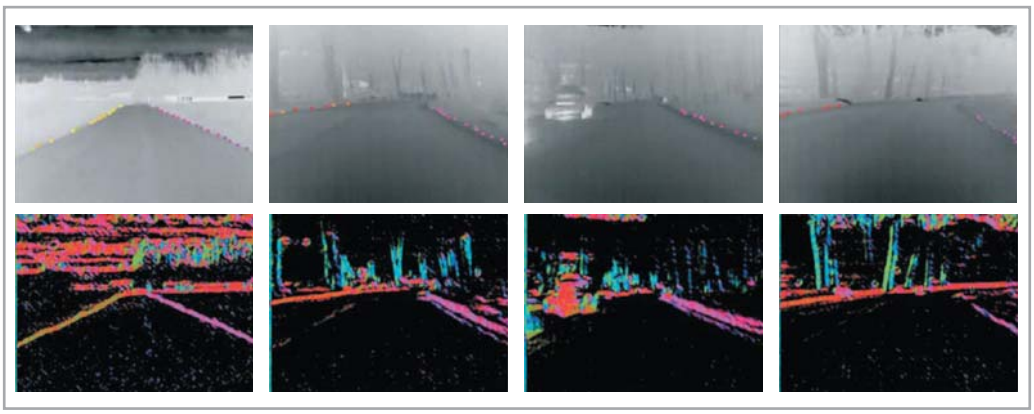

Fig. 8 Examples of the processed FIR images and the corresponding tracking results

＜著　者＞

高木　聖和
（たかぎ　きよかず）
研究開発３部
レーザレーダを使った環境認識技術の開発に従事

Basel　Fardi
（バーゼル　ファルディ）
FusionSystems GmbH　工学博士
画像処理，物体識別技術の研究開発に従事

Hendrik　Weigel
（ヘンドリック　ヴァイゲル）
Chemnitz 工科大学　情報工学科
コンピュータビジョン，環境認識，運転支援システムの研究に従事

Gerd　Wanielik
（ゲルド　ヴァニーリック）
Chemnitz 工科大学
情報工学科教授　工学博士
センサフュージョン，通信システム，ナビゲーションシステムの研究に従事